Adatom Extraction from Pristine Metal Terraces by Dissociative Oxygen Adsorption: Combined STM and Density Functional Theory Investigation of O/Ag(110)

Jagriti Pal,[1,2] Takat B. Rawal,[3] Marco Smerieri,[1] Sampyo Hong,[4] Matti Alatalo,[5] Letizia Savio,[1] Luca Vattuone,[1,2] Talat S. Rahman,[3] and Mario Rocca[1,2]
[1]*IMEM-CNR, UOS Genova, Via Dodecaneso 33, 16146 Genova, Italy*
[2]*Dipartimento di Fisica, Università di Genova, Via Dodecaneso 33, 16146 Genova, Italy*
[3]*Department of Physics, University of Central Florida, Orlando, Florida 32816, USA*
[4]*Division of Physical Sciences, Brewton-Parker College, Mount Vernon, Georgia 30445, USA*
[5]*Center of Molecular Materials, Faculty of Science, P.O. Box 8000, FI-90400 University of Oulu, Finland*
(Received 18 November 2015; revised manuscript received 10 November 2016; published 1 June 2017)

The reconstruction and modification of metal surfaces upon O_2 adsorption plays an important role in oxidation processes and in gauging their catalytic activity. Here, we show by employing scanning tunneling microscopy and the *ab initio* density functional theory that Ag atoms are extracted from pristine (110) terraces upon O_2 dissociation, resulting in vacancies and in Ag-O complexes. The substrate roughening generates undercoordinated atoms and opens pathways to the Ag subsurface layer. With increasing O coverage, multiple vacancies give rise to remarkable structures. The mechanism is expected to be very general depending on the delicate interplay of energy and entropy, so that it may be active for other materials at different temperatures.

DOI: 10.1103/PhysRevLett.118.226101

Most metallic surfaces reconstruct upon dissociative O_2 adsorption. Such rearrangements of the surface, bearing an enormous importance in determining the catalytic activity in oxidative environments, consist most often in the formation of added rows of oxygen and metal atoms. The source of substrate atoms needed for the reconstruction has been heavily debated. The currently accepted mechanism is that they are released from preexisting step edges and diffuse eventually to the terraces, where they react with oxygen atoms generated by dissociation of O_2 impinging from the gas phase [1–3]. Evidence for this mechanism comes from the retraction of step edges of the substrate terraces upon oxidation, observed under controlled ultrahigh vacuum conditions, e.g., for Cu [2–5]. At odds with this explanation, scanning tunneling microscopy (STM) investigations show also added rows located in the middle of terraces [6,7], far away from atomic steps. Oxidation induces, moreover, surface roughening with the formation of pits, as reported for both Ag [8,9] and Cu [10]. For the latter case, an excavation of the substrate to produce the adatoms needed for the reconstruction was suggested to dominate when the supply from steps is inhibited, albeit without unraveling the mechanism.

We show here that Ag atom excavation occurs on Ag(110) already at a sample temperature $T < 200$ K, leading to single vacancy formation or to more complex structures depending on atomic oxygen coverage, Θ_O. Density functional theory (DFT) based calculations allow us to describe the detailed mechanisms involved in the extraction process.

Silver bears a special importance in this context, since it is a unique catalyst for industrially relevant but not completely understood reactions [11,12]. Thus, oxygen adsorption on Ag surfaces continues to be the subject of thorough investigations and a paradigm for understanding the initial stages of oxidation. The tremendous complexity of an apparently simple system led to conflicting results [see, e.g., the debate about the surface oxide vs chemisorbed nature of Ag(111)-(4×4) O [13,14]]. Eventually, it became clear that the O atoms may end up in a variety of super- and subsurface sites [15–19], induce various types of substrate reconstructions, and cause the nucleation of different surface oxide phases [20]. In addition, the ease by which oxygen penetrates into the Ag subsurface region already at low T is puzzling. Not surprisingly, the role of subsurface O was invoked in catalytic processes at Ag surfaces [12,17,18]. Segregation and dissolution were monitored by photoemission spectroscopy for different Ag surfaces [21,22]. In particular, for O_2/Ag(110) some observations remained so far unexplained.

(a) The outermost Ag(110) plane is known to undergo disordering upon thermal O_2 dissociation at 150 K as evidenced by a severe drop in the elastic reflectivity of the low energy electron beam used in high resolution electron energy loss spectroscopy (HREELS) [23]. Broad EEL peaks, extending from 30 to 40 meV, indicate a strong surface inhomogeneity and the presence of several oxygen species. Two of them were shown to be reactive to CO dosed by a supersonic molecular beam (SMB) in titration experiments, while others must be unreactive since not all surface O is removed in the reaction [24,25]. The electron reflectivity recovers to normal values only at $T \sim 200$ K, when the added-row reconstruction forms [23].

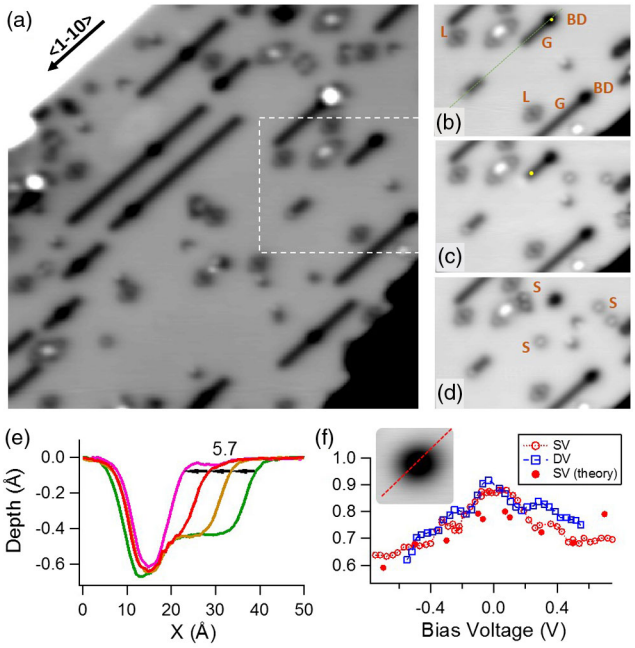

FIG. 1. (a) STM image (250 Å × 250 Å) recorded after an exposure of 19 L of O_2 on Ag(110) at 175 K by backfilling. (b)–(d) Images of the area delimited by the rectangle in (a). Size, 120 Å × 82 Å. The sequence shows the effect of vertical manipulation on the gray lines: Voltage pulses (at the yellow dots) generate two sombreros (S) and the corresponding shortening of the structure by two lattice spacings (STM images were recorded at 6 K, $V = 70$ mV). (e) Line profiles of BD and G along $[1\bar{1}0]$ [dotted line in (b)] recorded at different stages of the manipulation process. (f) Apparent depth vs bias voltage for BD corresponding to SV or DV. For SV, a comparison with simulated STM images is shown. Inset enlargement of a BD with line scans used to determine the depth.

(b) At the nanoscale, STM investigations [26,27] evidenced a variety of O-related features for 150 K < T < 190 K. The relative abundance of these features depends much on the surface preparation procedure. In the low coverage limit, slight rhombus-shaped (lozenges) and deep circular indentations (black holes) [26,27] are predominant. If O_2 is dosed directly at 175 K, as in Ref. [27], additional mobile sombrero-shaped objects are present, identical to those formed when O_2 dissociation is induced at 11 K by electron injection through the STM tip [28,29]. Similarly, sombrero-shaped O adatoms were observed also on Ag(001) upon brief O_2 exposure at 200 K [30] and assigned by STM image simulation.

In the present study, the O_2 uptakes have been performed either by backfilling or by SMB. Since the O_2 sticking probability is large at hyperthermal energy [19,24,31], the SMB enables performing clean experiments at coverages precluded to back-filling conditions [31,32]. Details about the experimental protocol and the DFT calculations for the energetics and simulation of STM images can be found in Supplemental Material [33].

Figure 1(a) shows a typical STM overview of the Ag(110) surface after a short O_2 exposure at 175 K. The coverage, evaluated *a posteriori* by counting the O-containing objects present in several images, is ~0.02 ML, so that all features are well isolated. Lozenges [marked L in Fig. 1(b)], gray tails (G), and black dots (BD) are visible as depressions 0.25, 0.4 and 0.6–0.8 Å deep, respectively, at a bias $V = 70$ mV. BD and G are located on top of Ag rows by taking as a reference atomically resolved added rows coexisting on the surface (see Fig. S1 in [33]).

Gray features are imaged only at a low tip voltage (+70 mV), and their bias dependence indicates that they contain O atoms. Most of them are arranged in segments aligned along $[1\bar{1}0]$ starting from a black dot. When a low voltage pulse (70 mV, 200 msec, 1 nA) is applied either to the black dot or to its tail (sequence b–d), the latter shortens from its free end by ~5.7 Å [see line scans in Fig. 1(e)], i.e., by two lattice spacings along $[1\bar{1}0]$. Simultaneously, two sombrero-shaped objects are generated [marked S in Fig. 1(d) and located in long bridge sites]. Also, sombreros are imaged only at a low bias (±70 mV). In accord with the literature, we ascribe them to O adatoms [26–29].

The elongated gray structure could be completely destroyed by repeated vertical manipulation, until an isolated BD is retrieved. In this case, the structure is perfectly round, with a highly symmetric depth profile [pink trace in Fig. 1(e)] centered at an Ag lattice site. Sometimes, on the contrary, BDs have a prolate shape and are centered on short bridge sites. In both cases, there is little bias dependence [see Fig. 1(f)], which suggests that they are single (SV) and double (DV) Ag vacancies, respectively, and not O-containing features.

The statistical relevance of the dissociation process is demonstrated by its absolute reproducibility, tested over five gray rows. Overall, 22 sombreros were generated in a controlled way from the gray rows by short voltage pulses. By subsequent voltage pulses, the so-generated sombreros could be displaced, merged into gray or black and white features, and separated again.

These experimental evidences are corroborated by simulated STM images [Figs. 2(d)–2(f)], corresponding to the DFT optimized geometries shown in Figs. 2(a)–2(c). Oxygen at a long bridge (LB) site [Figs. 2(a),2(d), and 2(g)] appears as a sombrero-shaped depression of 0.25 Å in the STM image simulated for 70 mV, confirming our empirical assignment of this object. Its apparent depth becomes shallower at ±0.7 V (not shown), in agreement with experiment [27]. The single Ag vacancy [Figs. 2(b), 2(e), and 2(h)] appears as a depression of ~0.8 Å, corresponding to a black dot in the STM images simulated for 70 and 700 mV. O adatoms in threefold hollows (TFH) [Figs. 2(c),2(f), and 2(i)] appear as a depression of ~0.4 Å in the STM image simulated for 70 mV; they form zigzag chains at the opposite side of a vertically displaced Ag row. This structure is thus a good candidate for the elongated

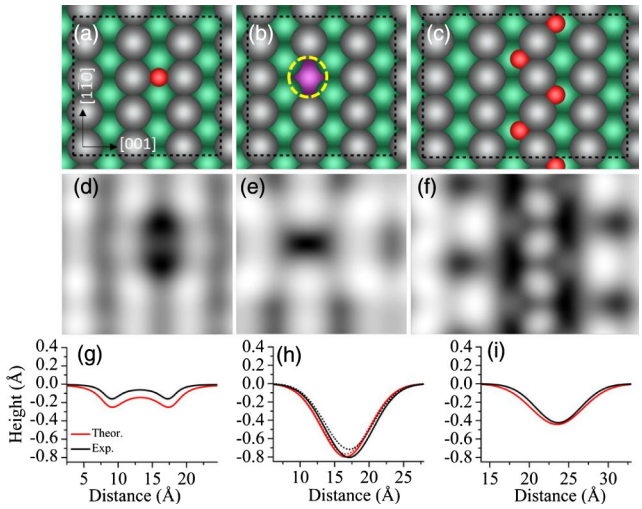

FIG. 2. (a)–(c) DFT-optimized geometries and (d)–(f) simulated STM images (at 70 mV) of (a),(d) O in LB (S), (b),(e) Ag vacancy (BD), and (c),(f) O atoms in threefold hollows, forming a zigzag chain on Ag(110) (G). (g)–(i) Comparison of theoretical (red trace) and experimental (black trace) depth profiles for $V = 70$ mV. They are obtained from line scans, along $[1\bar{1}0]$ for (d) and (e) and along [001] for (f). To allow a comparison with the experiment, the calculated profiles were convoluted with a suitable function simulating the tip. A small dependence of the depth profile on the bias voltage is observed in the experimental data, in agreement with Fig. 1(f). Here and in the following, Ag atoms in the first, second, and third layers and O atoms are represented by gray, green, purple, and red balls, respectively.

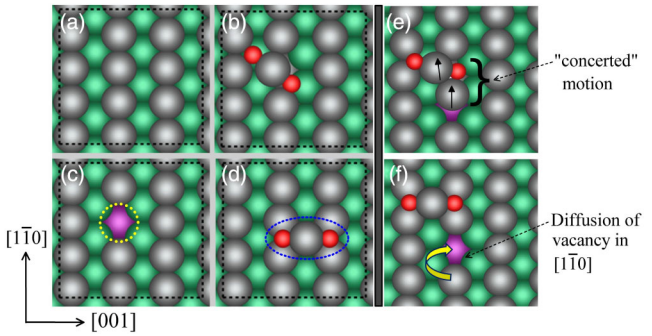

FIG. 3. Schematic representation for the formation of a single Ag vacancy and added O-Ag-O unit on Ag(110): (a) pristine surface; (b) the dissociated O atoms participate to form an O-Ag-O complex, resulting in a weakening of Ag-Ag bonds in the substrate; (c) Ag vacancy (yellow dotted line); (d) O-stabilized Ag adatom (blue dotted line); (e) diffusion of O-Ag-O complex and Ag atom in "concerted" motion; and (f) diffusion of the vacancy away from the added O-Ag-O complex.

gray tails in Fig. 1(a) and justifies why sombreros are produced in couples upon vertical manipulation: One unit of the zigzag row is disrupted and shortens by two lattice spacings along $[1\bar{1}0]$ ejecting two oxygens. Deeper indentations could be obtained only by removing substrate atoms and creating Ag vacancies.

In the absence of oxygen, vacancy formation cannot be observed, since extracted Ag atoms most likely refill the just-created vacancy. Indeed, DFT results show that (i) the formation energy of an Ag vacancy plus Ag adatom on pristine Ag(110) is 0.42 eV, (ii) the energy barrier for this process to occur is 0.69 eV, whereas the reverse barrier is 0.27 eV (see Fig. S3a), and (iii) such a value is much lower than the barrier of 0.47 eV for the diffusion of the Ag vacancy along $[1\bar{1}0]$ (see Fig. S2). Ag vacancy creation and adatom formation on bare Ag(110) occurs thus only for $T > 750$ K [40].

In the presence of oxygen atoms, vacancy formation on Ag(110) becomes possible (see Fig. 3), since the formation energy $E_v^{ad,\text{O-Ag-O}}$ is reduced to 0.055 eV. If E_a to E_d are the total energies for the structures shown in Figs. 3(a)–3(d), respectively, we have

$$E_v^{ad,\text{O-Ag-O}} = -\{(E_a + E_b) - (E_c + E_d)\}.$$

The formation of an Ag vacancy [Fig. 3(c)] *plus* an oxygen-decorated Ag adatom [added O-Ag-O unit, Fig. 3(d)] is thus only slightly endothermic and may take place thanks to the entropic contribution to the free energy. The barrier for the formation of an Ag vacancy plus added O-Ag-O unit reduces to 0.52 eV for the "concerted motion" [Fig. 3(e)] in which the -OAg-O complex of Fig. 3(b) diffuses to the nearest neighboring hollow (H) site dragging also the Ag atom in the $[1\bar{1}0]$ direction [see also Fig. S3(b)]. With increasing O coverage, the barrier decreases to 0.46 eV (see Fig. S4). The reverse barrier increases substantially, thus inhibiting the vacancy-destruction process. Once formed, the vacancy diffuses therefore away from the O-decorated Ag adatom [see Fig. 3(f)], avoiding recombination (see discussion of Fig. S2), leading to the isolated vacancy [Fig. 3(c)] and the O-decorated Ag adatom [Fig. 3(d)].

Dissociation of O_2 with the production of two O atoms is exothermic with an energy barrier of 0.42 eV [41]. Our kinetic Monte Carlo (KMC) simulations show that this process is peaked around 157 K (Fig. S5 in [33]), in good agreement with the experimental value of 150 K. Then, the O-Ag-O complex in Fig. 3(b) forms spontaneously, since it is energetically favored by 70 meV with respect to two oxygen atoms at H sites two lattice spacings apart. In STM, such a complex is imaged by a gray dot with a whitish side along $[1\bar{1}0]$ which has indeed been sporadically observed in our images (Figs. S6 and S7 in [33]). The complexes formed at 175 K merge together into the gray chains attached to the Ag vacancy. Finally, for vacancy formation, the system needs to overcome the previously discussed barrier of 0.52 eV. The KMC simulation (Fig. S5 in [33]) indicates that the latter process is peaked at 185–190 K at low O coverage (decreasing with increasing coverage). The relative

populations of O-Ag-O complexes and vacancies will thus depend on T and O coverage.

The system then has to cope with the 55 meV endothermicity of the internal energy balance. Such a difference can be compensated by the entropic contribution to the free energy (calculated to be ~ 1 meV/K for a square Ag lattice [42]). Vacancy formation is thus possible only above 60 K. Indeed, no vacancy formation was observed by Hahn and Ho [28,29] in their O_2 disruption experiments performed at 13 K.

Figures 4(a) and 4(b) show STM images of an O/Ag(110) surface obtained by dosing O_2 with the SMB, corresponding to an estimated O coverage of 0.06 ML. During exposure, T was kept at either 165 or 185 K [Figs. 4(a) and 4(b), respectively]. Overcoming the limit of low coverage, more complex structures form in addition to the previously described ones. In particular, "butterfly-shaped" objects [see the enlargement in Fig. 4(c)] are now present. They appear as elongated depressions along $[1\bar{1}0]$, ending at both extremities with a round protrusion sided laterally by "wings." Butterflies are abundant at 175 K and at 185 K but rare when dosing O_2 at 165 K. To unravel this complex structure, we performed DFT calculations, modeling it with a pair of vacancies and with four oxygen atoms. As evident from Fig. 4(d), in the DFT-optimized geometry the two Ag atoms at the "head" and "tail" of the butterfly are displaced from their original site, and each one is sided by two O (see also the discussion on Fig. S9a and S10 in [43]). The simulated STM image [Fig. 4(e)] of the relaxed structure shows a remarkable agreement with the experiment. Notably, the energy of the couple of O is -2.9 eV, and the overall structure is asymmetric with respect to $[1\bar{1}0]$.

Multiple Ag vacancies are found to form following the dissociation of additional O_2 molecules. The orientation along $[1\bar{1}0]$ of such chains of vacancies is in accord with the anisotropy of the barrier for vacancy diffusion (see Fig. S2 in [33]). Indeed, at 175 K, vacancy migration is active only along the Ag rows. Moreover, attaching an additional vacancy to an already existing one results in energy gain (Fig. S8 in [33]). The process saturates eventually above three Ag vacancies, which compares nicely with the observed lengths of the body of the butterflies in Fig. 4.

The calculated barriers for vacancy formation imply that the relative abundance of black dots and sombreros depends on T and preparation conditions, explaining the different results present in the literature.

At low coverage, O-decorated Ag adatoms in Fig. 3(d) most probably end up at step edges, where they are difficult to be identified, while at high coverage they stick at the vacancies forming the wings. Statistically, some vacancies may be filled up by O-decorated complexes, and O atoms can then be buried into the Ag subsurface region, giving a rationale for the efficient subsurface migration already at low T.

Finally, the substrate reconstruction in Fig. 3(b) explains the strong disordering of the Ag(110) substrate upon O_2 dissociation at low T mentioned in the introduction [23]. Indeed, the Ag atoms forming the O-Ag-O complex undergo a vertical displacement of 0.56 Å. The drop in the reflected electron beam intensity is thereby largest at low electron kinetic energies, since the electrons are then reflected off the attractive potential barrier, which becomes heavily corrugated.

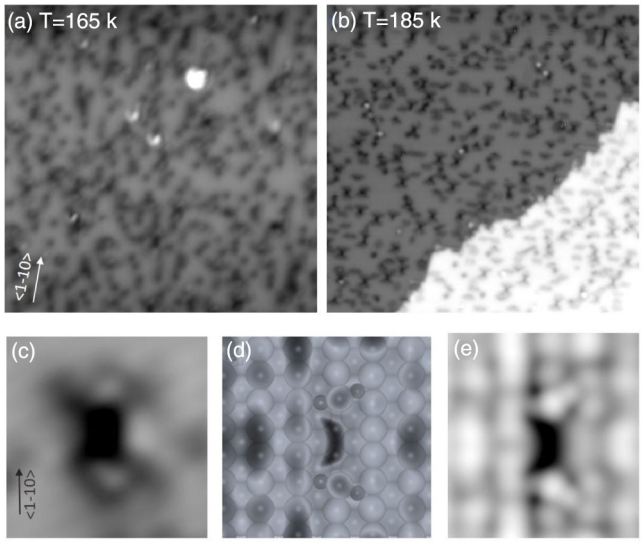

FIG. 4. (a),(b) STM images of O/Ag (110) after dosing O_2 at 0.4 eV kinetic energy by SMB, at $T = 165$ K (a) and $T = 185$ K (b). The estimated coverage is 0.06 ML. Image size 450 Å $\times$ 450 Å, $V = 70$ mV, $I = 1.0$ nA. (c) Enlargement of a butterfly structure (image size 34 Å $\times$ 33 Å, $V = 70$ mV). (d), (e) DFT-optimized geometry and simulated STM image of the butterfly unit. See Fig. S10 in Supplemental Material [33] for the atomic positions.

In conclusion, our combined STM investigation and DFT analysis of the O/Ag(110) system provides a detailed insight into the mechanisms involved in the process of vacancy formation. The latter is possible at pristine terraces only in the presence of O adatoms, and the process gets easier for the higher oxygen coverage, thus leading to butterfly formation. Further insight on the disruption mechanism could be gained by STM investigations with deliberate functionalization of the tip and subsequent simulations of the images.

Vacancy formation is remarkable for Ag(110) at 175 K, but it is expected to take place also for the other Ag surfaces, albeit at higher T, since more bonds need to be broken to extract Ag adatoms (see Fig. S11 in [33]). A similar scenario may occur also for other metals at high enough T, thus accounting for the still unexplained observations reported for Cu surfaces [10] and for Au(111) [43]. As we learned recently, vacancies form indeed for O/Ag(111) when O_2 is dosed at 433 K [44]. The so-generated adatoms constitute the building blocks for the added row reconstruction on Ag(110), providing the main supply of substrate atoms far from step edges or at low T. This explains thus the observed nucleation

of added rows also in the middle of wide terraces. The occurrence of vacancy excavation explains for the well-known facile access of oxygen to the Ag subsurface region.

Such properties are relevant for the understanding of the catalytic properties of Ag, in particular, and of noble metals, in general, since vacancies are undercoordinated and thus inherently reactive. A significant subsurface O content provides, moreover, a precious reservoir of reactants.

We thank Robert Reichelt, Rameez Ud Din, and Angelique Lusuan for helping in different phases of the experiment. We acknowledge the financial support by International Center for Theoretical Physics (ICTP) through a postdoctoral grant and of Compagnia San Paolo. We thank the STOKES Advanced Research Computing Center at the University of Central Florida, the Texas Advanced Computing Center (TACC), the National Energy Research Scientific Computing Center (NERSC), and the Center for Nanoscale Materials (CNM) of the Argonne National Laboratory for providing the computational resources. T. B. R., S. H., and T. S. R. thank Duy Le for fruitful discussion on simulated STM images and U.S. NSF for partial support under Grant No. CHE-1310327.

[1] F. Besenbacher and F. B. Nørskov, Prog. Surf. Sci. **44**, 5 (1993).
[2] D. J. Coulman, J. Wintterlin, R. J. Behm, and G. Ertl, Phys. Rev. Lett. **64**, 1761 (1990).
[3] F. Jensen, F. Besenbacher, E. Lægsgaard, and I. Stensgaard, Phys. Rev. B **41**, 10233 (1990).
[4] Q. Liu, L. Li, N. Cai, W. A. Saidi, and G. Zhou, Surf. Sci. **627**, 75 (2014).
[5] L. Li, N. Cai, W. A. Saidi, and G. Zhou, Chem. Phys. Lett. **613**, 64 (2014).
[6] T. Zambelli, J. V. Barth, and J. Wintterlin, Phys. Rev. B **58**, 12663 (1998).
[7] M. Taniguchi, K. Tanaka, T. Hashizume, and T. Sakurai, Surf. Sci. **262**, L123 (1992).
[8] W. W. Pai, N. C. Bartelt, and J. E. Reutt-Robey, Phys. Rev. B **53**, 15991 (1996).
[9] W. W. Pai, N. C. Bartelt, M. R. Peng, and J. E. Reutt-Robey, Surf. Sci. **330**, L679 (1995).
[10] L. D. Sun, M. Hohage, R. Denk, and P. Zeppenfeld, Phys. Rev. B **76**, 245412 (2007).
[11] *Handbook of Heterogeneous Catalysis*, edited by G. Ertl, H. Knoezinger, F. Schueth, and J. Weitkamp (Wiley-VCH Verlag, Weinheim, 2008).
[12] S. Böcklein, S. Günther, and J. Wintterlin, Angew. Chem., Int. Ed. **52**, 5518 (2013).
[13] J. Schnadt, A. Michaelides, J. Knudsen, R. T. Vang, K. Reuter, E. Lægsgaard, M. Scheffler, and F. Besenbacher, Phys. Rev. Lett. **96**, 146101 (2006).
[14] M. Schmid *et al.*, Phys. Rev. Lett. **96**, 146102 (2006).
[15] J. Schnadt, J. Knudsen, X. L. Hu, A. Michaelides, R. T. Vang, K. Reuter, Z. Li, E. Lægsgaard, M. Scheffler, and F. Besenbacher, Phys. Rev. B **80**, 075424 (2009).
[16] M. Rocca *et al.*, Phys. Rev. B **61**, 213 (2000).
[17] S. Günther, S. Böcklein, J. Wintterlin, M. A. Niño, T. O. Mentes, and A. Locatelli, Chem. Cat. Chem **5**, 3342 (2013).
[18] T. C. R. Rocha, A. Oestereich, D. V. Demidov, M. H. Vecker, S. Zafeiratos, G. Weinberg, V. I. Bukhtiyarov, A. Knop-Gericke, and R. Schlögl, Phys. Chem. Chem. Phys. **14**, 4554 (2012).
[19] L. Vattuone, L. Savio, and M. Rocca, Phys. Rev. Lett. **90**, 228302 (2003).
[20] L. Savio, C. Giallombardo, L. Vattuone, A. Kokalj, and M. Rocca, Phys. Rev. Lett. **101**, 266103 (2008).
[21] L. Savio, A. Gerbi, L. Vattuone, A. Baraldi, G. Comelli, and M. Rocca, J. Phys. Chem. B **110**, 942 (2006).
[22] M. Rocca *et al.*, Phys. Rev. B **63**, 081404 (2001).
[23] L. Vattuone, M. Rocca, P. Restelli, M. Pupo, C. Boragno, and U. Valbusa, Phys. Rev. B **49**, 5113 (1994).
[24] U. Burghaus and H. Conrad, Surf. Sci. **338**, L869 (1995).
[25] U. Burghaus and H. Conrad, Surf. Sci. **370**, 17 (1997).
[26] T. Zambelli, J. V. Barth, and J. Wintterlin, J. Phys. Condens. Matter **14**, 4241 (2002).
[27] M. Smerieri, L. Savio, L. Vattuone, and M. Rocca, J. Phys. Condens. Matter **22**, 304015 (2010).
[28] J. R. Hahn and W. Ho, J. Chem. Phys. **122**, 244704 (2005).
[29] J. R. Hahn and W. Ho, J. Chem. Phys. **123**, 214702 (2005).
[30] S. Schintke, S. Messerli, K. Morgenstern, J. Nieminen, and W.-D. Schneider, J. Chem. Phys. **114**, 4206 (2001).
[31] L. Vattuone, M. Rocca, C. Boragno, and U. Valbusa, J. Chem. Phys. **101**, 726 (1994).
[32] I. Lončarić, M. Alducin, and J. I. Juaristi, Phys. Chem. Chem. Phys. **17**, 9436 (2015).
[33] See Supplemental Material at http://link.aps.org/supplemental/10.1103/PhysRevLett.118.226101 for further details, which includes Refs. [34–39].
[34] M. Smerieri, R. Reichelt, L. Savio, L. Vattuone, and M. Rocca, Rev. Sci. Instrum. **83**, 093703 (2012).
[35] J. M. Blanco *et al.*, Phys. Rev. B **71**, 113402 (2005).
[36] I. Horcas, R. Fernández, J. M. Gómez-Rodríguez, J. Colchero, J. Gómez-Herrero, and A. M. Baro, Rev. Sci. Instrum. **78**, 013705 (2007).
[37] J. Tersoff and D. R. Hamann, Phys. Rev. Lett. **50**, 1998 (1983).
[38] G. Henkelman, B. P. Uberuaga, and H. Jonsson, J. Chem. Phys. **113**, 9901 (2000).
[39] P. Stoltze, J. Phys. Condens. Matter **6**, 9495 (1994).
[40] T. S. Rahman, Z. Tian, and J. E. Black, Surf. Sci. **374**, 9 (1997).
[41] T. B. Rawal, S. Hong, A. Pulkkinen, M. Alatalo, and T. S. Rahman, Phys. Rev. B **92**, 035444 (2015).
[42] A. Savara, J. Phys. Chem. C **117**, 15710 (2013).
[43] B. K. Min, X. Deng, D. Pinnaduwage, R. Shalek, and C. M. Friend, Phys. Rev. B **72**, 121410(R) (2005).
[44] B. V. Andryushechkin, V. M. Shevlyuga, T. V. Pavlova, G. M. Zhidomirov, and K. N. Eltsov, Phys. Rev. Lett. **117**, 056101 (2016).